[2]Jiang, G.-S., and Shu, C.-W., "Efficient Implementation of Weighted ENO Schemes," *Journal of Computational Physics*, Vol. 126, No. 1, 1996, pp. 202–228.

[3]Harten, A., Engquist, B., Osher, S., and Chakravarthy, S., "Uniformly High-Order Accurate Nonoscillatory Scheme, III," *Journal of Computational Physics*, Vol. 71, No. 2, 1987, pp. 231–303.

[4]Shu, C.-W., and Osher, S., "Efficient Implementation of Nonoscillatory Shock Capturing Schemes," *Journal of Computational Physics*, Vol. 77, No. 2, 1988, pp. 439–471.

[5]Perng, Y. C., Yen, R. H., and Yang, J. Y., "Implicit Weighted ENO Schemes for the Euler Equations," *Computational Fluid Dynamics Journal*, Vol. 8, No. 3, 1999, pp. 216–227.

[6]Yoon, S., and Jameson, A., "Lower-Upper Symmetric-Gauss-Seidel Method for the Euler and Navier–Stokes Equations," *AIAA Journal*, Vol. 26, No. 8, 1988, pp. 1025, 1026.

[7]Chakravarthy, S. R., and Ota, O. K., "Numerical Issues in Computing Inviscid Supersonic Flow over Conical Delta Wing," AIAA Paper 86-0440, Jan. 1986.

[8]Kandil, O. A., and Chuang, A., "Influence of Numerical Dissipation on Computational Euler Solutions for Conical Vortex Dominated Flows," *AIAA Journal*, Vol. 25, No. 6, 1987, pp. 1426–1434.

[9]Barth, T. J., "A 3-D Upwind Euler Solver for Unstructured Meshes," 10th AIAA Computational Fluid Dynamics Conf., AIAA Paper 91-1548-CP, June 1991.

[10]McAlister, K. W., and Takahashi, R. K., "NACA 0015 Wing Pressure and Trailing Vortex Measurements," USAAVSCOM TR-91-A-003, NASA Ames Research Center, CA, March 1991.

[11]Schmitt, V., and Charpin, F., "Pressure Distributions on the ONERA-M6 Wing at Transonic Mach Numbers," AGARD-AR-138- B1, NATO, Aug. 1979.

[12]Yoon, S., Jameson, A., and Kwak, D., "Effect of Artificial Diffusion Schemes on Multigrid Convergence," 12th AIAA Computational Fluid Dynamics Conf., AIAA Paper 95-1670-CP, June 1995.

[13]Wardlaw, A. B., Jr., and Davis, S. F., "Euler Solutions for Delta Wings," *AIAA Journal*, Vol. 28, No. 7, 1990, pp. 1826–1829.

Propeller Momentum Theory with Slipstream Rotation

W. F. Phillips*
Utah State University, Logan, Utah 84322-4130

Introduction

ONE critical component of propeller blade element theory[1] is the prediction of the velocity induced on the propeller disk as a result of the lift developed by the blades. Two methods are commonly used to predict this induced velocity. The most comprehensive method is Goldstein's vortex theory.[2] The simplest method is propeller momentum theory,[3–5] which is the topic addressed here. The major objection to the use of classical propeller momentum theory has been its failure to account for the rotation of the fluid within the slipstream.

Classical propeller momentum theory is presented in most aeronautical engineering textbooks that deal with propeller performance.[3–5] Momentum theory is based on the hypothesis of a streamtube, which encloses the complete propeller disk as shown in Fig. 1. This streamtube is assumed to extend from a plane infinitely far upstream from the propeller disk to a plane infinitely far downstream. All of the fluid that enters this streamtube on the far upstream side must pass through the propeller disk and exit the streamtube on the far downstream side.

Received 22 February 2001; revision received 1 October 2001; accepted for publication 7 October 2001.

*Professor, Mechanical and Aerospace Engineering Department, 4130 Old Main Hill. Member AIAA.

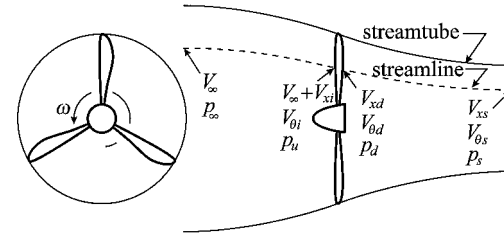

Fig. 1 Momentum theory model for the pressures and velocities of the fluid that flows through the disk of a rotating propeller, including the effects of fluid rotation.

In addition to the foundation hypothesis of streamtube flow shown in Fig. 1, classical propeller momentum theory imposes five simplifying approximations. The flow is assumed to be 1) inviscid and 2) incompressible; 3) all rotation of the fluid within the streamtube is neglected; and both 4) the velocity and 5) the static pressure are assumed uniform over each cross section of the streamtube. With these approximations the induced velocity V_i is expressed as a function of the freestream velocity V_∞ and the thrust T. In dimensionless form the result is

$$\frac{V_i}{(\omega/2\pi)d_p} = \sqrt{\frac{J^2}{4} + \frac{2C_T}{\pi}} - \frac{J}{2} \tag{1}$$

where $C_T \equiv T/[\rho(\omega/2\pi)^2 d_p^4]$ and $J \equiv V_\infty/[(\omega/2\pi)d_p]$ are the usual thrust coefficient and advance ratio. Here, ω is used to represent the propeller angular velocity, d_p is the propeller diameter, and ρ is the fluid density. From the same analysis the propulsive efficiency for the propeller is found to be

$$\eta_i \equiv TV_\infty/Q\omega = \left(\tfrac{1}{2} + \sqrt{\tfrac{1}{4} + 2C_T/\pi J^2}\right)^{-1} \tag{2}$$

where Q is the torque required to turn the propeller and η_i is usually called the ideal propulsive efficiency.

The major objection to these results has been the failure of the method to account for rotation of the fluid within the slipstream. There appears to be no physical basis for neglecting slipstream rotation. Clearly, torque must be applied to turn the propeller and that torque must result in rotation of the fluid within the slipstream. Because some of the power supplied to the propeller must go to support this rotation, the propulsive efficiency will be reduced as a result of slipstream rotation. In the following analysis we shall examine the magnitude of this effect.

Effects of Slipstream Rotation

We shall now consider the incorporation of the angular momentum equation into the model hypothesized in propeller momentum theory. To isolate the effects of slipstream rotation, we will continue with the assumptions of inviscid, incompressible, uniform flow, but we will now allow for rotation of the fluid within the streamtube. Accordingly, we will continue to assume the existence of a streamtube, which encloses the complete propeller disk as shown in Fig. 1. This streamtube is still assumed to extend infinitely far upstream from the propeller disk, to a plane where the static pressure is constant and equal to the freestream static pressure p_∞. In this plane the axial velocity is the freestream velocity V_∞, and there is no circumferential velocity. Likewise, the streamtube is assumed to extend infinitely far downstream from the propeller disk to a plane where the velocity in the slipstream is no longer changing in the axial direction. Consistent with the uniform flow assumption used in classical propeller momentum theory, we will continue to assume uniform axial velocity but will now allow for a uniform angular velocity as well. Because we wish to examine the effect of slipstream rotation on the results predicted by propeller momentum theory, at first thought one might be tempted to continue with the assumption of uniform pressure, which is also imposed in classical propeller momentum theory. However, this assumption is not consistent with rotation in the ultimate slipstream.

The solution obtained from classical propeller momentum theory does not satisfy the angular momentum equation. If we continue with the uniform pressure assumption from classical momentum theory while allowing for fluid rotation, we find that there is only one possible case for which the angular momentum equation together with the other laws of Newtonian mechanics can all be satisfied with a finite propeller rotational speed. That is the case of zero thrust. Because we are now allowing for fluid rotation in the streamtube and we wish to consider a propeller developing finite thrust, we can no longer assume uniform pressure over each cross section of the streamtube. We must instead allow the pressure in the streamtube to be a function of the radial position r, as well as the axial position x.

On the near upstream side of the propeller disk, the axial fluid velocity is equal to the sum of the forward airspeed and the axial component of induced velocity $V_\infty + V_{\mathrm{xi}}$. On the near downstream side of the propeller disk, the axial fluid velocity is designated V_{xd}. The circumferential velocity on the near upstream side of the propeller disk is just the circumferential component of the propeller induced velocity $V_{\theta i}$, and the circumferential velocity on the near downstream side of the propeller disk is denoted as $V_{\theta d}$.

The circumferential component of fluid velocity just upstream from the propeller disk can be deduced by applying the angular momentum equation to the section of streamtube that is upstream from the propeller. Because there is no torque acting on this section of the streamtube, there can be no change in the angular momentum of the air as it passes through this section. Because the air has no angular momentum far upstream from the propeller disk, it cannot have angular momentum when it reaches the upstream side of the propeller disk. This requires

$$V_{\theta i} = 0 \tag{3}$$

and thus

$$V_{\mathrm{xi}} = V_i \tag{4}$$

The axial component of fluid velocity just downstream from the propeller disk is related to the axial component on the upstream side through the continuity equation. If we use the notation shown in Fig. 1 and apply conservation of mass across any segment of the propeller disk, for the assumed incompressible flow we have

$$V_{\mathrm{xd}} = V_\infty + V_i \tag{5}$$

The pressure and velocity just upstream from the propeller disk are related to the freestream pressure and velocity through Bernoulli's equation. Applying Bernoulli's equation along the streamline shown in Fig. 1 and using Eqs. (3) and (4), upstream from the propeller disk we obtain

$$\frac{p_\infty}{\rho} + \frac{V_\infty^2}{2} = \frac{p_u}{\rho} + \frac{(V_\infty + V_i)^2}{2} \tag{6}$$

Here we see that because there is no rotation of the fluid in the upstream section of the streamtube the uniform flow approximation requires uniform pressure upstream from the propeller disk. For the streamline on the aft side of the propeller disk, from a point just behind the propeller to a point in the far slipstream using Eq. (5) we can write

$$\frac{p_s}{\rho} + \frac{V_{\mathrm{xs}}^2 + V_{\theta s}^2}{2} = \frac{p_d}{\rho} + \frac{(V_\infty + V_i)^2 + V_{\theta d}^2}{2} \tag{7}$$

where V_{xs} and $V_{\theta s}$ are the axial and circumferential components of velocity in the ultimate slipstream.

Subtracting Eq. (6) from Eq. (7) and expressing the circumferential velocity in the ultimate slipstream as the product of the local angular velocity and the local radius, we have

$$\frac{p_s}{\rho} - \frac{p_\infty}{\rho} + \frac{V_{\mathrm{xs}}^2 + \omega_s^2 r_s^2}{2} - \frac{V_\infty^2}{2} = \frac{p_d}{\rho} - \frac{p_u}{\rho} + \frac{V_{\theta d}^2}{2} \tag{8}$$

where ω_s and r_s are the angular velocity and radial coordinate at the location of the streamline far downstream from the propeller.

In the ultimate slipstream this axisymmetric flow becomes independent of the axial position x. Thus, the continuity equation in the ultimate slipstream requires

$$\frac{\mathrm{d}(r_s V_{\mathrm{rs}})}{\mathrm{d}r_s} = 0$$

where r_s is the radial position and V_{rs} is the radial velocity at a point in the ultimate slipstream. Similarly, the radial component of the momentum equation in the ultimate slipstream reduces to

$$\rho\left(V_{\mathrm{rs}}\frac{\mathrm{d}V_{\mathrm{rs}}}{\mathrm{d}r_s} - \frac{V_{\theta s}^2}{r_s}\right) = -\frac{\mathrm{d}p_s}{\mathrm{d}r_s}$$

The solution to these two equations subject to the boundary conditions of freestream static pressure and zero radial velocity at the outer edge of the slipstream $r_s = R_s$ gives

$$p_s(r_s) = p_\infty - \left(\rho\omega_s^2/2\right)\left(R_s^2 - r_s^2\right) \tag{9}$$

Using Eq. (9) in Eq. (8) results in

$$\omega_s^2\left(r_s^2 - \frac{R_s^2}{2}\right) + \frac{V_{\mathrm{xs}}^2}{2} - \frac{V_\infty^2}{2} = \frac{p_d}{\rho} - \frac{p_u}{\rho} + \frac{V_{\theta d}^2}{2} \tag{10}$$

Applying the continuity equation to the flow inside the stream surface that contains the streamline under consideration, we obtain

$$r_s^2 = [(V_\infty + V_i)/V_{\mathrm{xs}}]r_p^2 \tag{11}$$

where r_p is the radial position of the streamline at the propeller. Using Eq. (11) in Eq. (10) yields

$$\omega_s^2\left(r_p^2 - \frac{R_p^2}{2}\right)\frac{V_\infty + V_i}{V_{\mathrm{xs}}} + \frac{V_{\mathrm{xs}}^2}{2} - \frac{V_\infty^2}{2} = \frac{p_d}{\rho} - \frac{p_u}{\rho} + \frac{V_{\theta d}^2}{2} \tag{12}$$

where R_p is the propeller's outside radius.

Because angular momentum remains constant downstream from the propeller, in view of Eq. (11) we have

$$V_{\theta d} = (r_s/r_p)V_{\theta s} = \left(r_s^2/r_p\right)\omega_s = [(V_\infty + V_i)/V_{\mathrm{xs}}]r_p\omega_s \tag{13}$$

After applying Eq. (13), Eq. (12) can be written as

$$\frac{p_d}{\rho} - \frac{p_u}{\rho} = \omega_s^2\left[\left(1 - \frac{V_\infty + V_i}{2V_{\mathrm{xs}}}\right)r_p^2 - \frac{R_p^2}{2}\right]\frac{V_\infty + V_i}{V_{\mathrm{xs}}} + \frac{V_{\mathrm{xs}}^2}{2} - \frac{V_\infty^2}{2} \tag{14}$$

The axial velocity in the ultimate slipstream is related to the thrust through the axial momentum equation

$$T + \int_{r_s=0}^{R_s}(p_\infty - p_s)2\pi r_s\,\mathrm{d}r_s = \int_{r_s=0}^{R_s}(V_{\mathrm{xs}} - V_\infty)\rho V_{\mathrm{xs}}2\pi r_s\,\mathrm{d}r_s$$

In view of Eq. (9), this is easily integrated and, after applying Eq. (11), we have

$$T = \pi R_p^2\rho\left\{(V_\infty + V_i)(V_{\mathrm{xs}} - V_\infty) - [(V_\infty + V_i)/2V_{\mathrm{xs}}]^2\omega_s^2 R_p^2\right\} \tag{15}$$

Because there is no change in axial velocity across the propeller disk, the thrust can also be expressed as

$$T = \int_{r_p=0}^{R_p}(p_d - p_u)2\pi r_p\,\mathrm{d}r_p$$

With Eq. (14) this is readily integrated to yield

$$T = \pi R_p^2\rho\left\{V_{\mathrm{xs}}^2/2 - V_\infty^2/2 - [(V_\infty + V_i)/2V_{\mathrm{xs}}]^2\omega_s^2 R_p^2\right\} \tag{16}$$

Eliminating the thrust with Eqs. (15) and (16) and solving for the axial velocity in the ultimate slipstream gives

$$V_{xs} = V_\infty + 2V_i \tag{17}$$

The rotation in the ultimate slipstream is related to the propeller torque through the angular momentum equation. After applying Eq. (11), this results in

$$Q = \int_{r_s=0}^{R_s} r_s^2 \omega_s (\rho V_{xs} 2\pi r_s \, dr_s) = \frac{\pi}{2} \rho V_{xs} \omega_s R_s^4$$

$$= \pi\rho \frac{(V_\infty + V_i)^2}{2V_{xs}} \omega_s R_p^4 \tag{18}$$

The brake power required to turn the propeller must satisfy the energy equation for incompressible flow

$$\omega Q = \int_{r_s=0}^{R_s} \left(\frac{p_s}{\rho} - \frac{p_\infty}{\rho} + \frac{V_{xs}^2 + \omega_s^2 r_s^2}{2} - \frac{V_\infty^2}{2} \right) \rho V_{xs} 2\pi r_s \, dr_s$$

Applying Eq. (9), integrating, and then applying Eq. (11), this gives

$$\omega Q = \pi R_p^2 \rho (V_\infty + V_i)\left(V_{xs}^2/2 - V_\infty^2/2 \right) \tag{19}$$

Combining Eqs. (18) and (19) to eliminate the torque, we can solve for the angular velocity in the ultimate slipstream. After using Eq. (17) to eliminate the axial component of the ultimate slipstream velocity, we have

$$\omega_s = \frac{4(V_\infty + 2V_i)V_i}{\omega R_p^2} \tag{20}$$

Applying Eqs. (17) and (20) to either Eq. (15) or (16), the thrust developed by the propeller is expressed as

$$T = 2\pi R_p^2 \rho (V_\infty + V_i) V_i \left[1 - \frac{2(V_\infty + V_i)V_i}{\omega^2 R_p^2} \right] \tag{21}$$

Likewise, using Eqs. (17) and (20) with either Eq. (18) or (19), the propeller brake power can be expressed as

$$\omega Q = 2\pi R_p^2 \rho (V_\infty + V_i)^2 V_i \tag{22}$$

Equation (21) is quadratic in $(V_\infty + V_i)V_i$ and can be directly solved for this velocity product. The result is quadratic in V_i and can be solved for the induced velocity. This gives

$$V_i = -\frac{V_\infty}{2} \pm \sqrt{\frac{V_\infty^2}{4} + \frac{\omega^2 R_p^2}{4} \left(1 \pm \sqrt{1 - \frac{4T}{\pi\rho\omega^2 R_p^4}} \right)}$$

In the limit as the rotational speed of the propeller becomes very large, for finite positive thrust the induced velocity must be positive and finite. This specifies the signs in the preceding relation. After nondimensionalizing we have

$$\frac{V_i}{(\omega/2\pi)d_p} = \sqrt{\frac{J^2}{4} + \frac{\pi^2}{4}\left(1 - \sqrt{1 - \frac{16C_T}{\pi^3}} \right)} - \frac{J}{2} \tag{23}$$

Similarly, using Eqs. (21) and (22) together with Eq. (23), the ideal propulsive efficiency can be written as

$$\eta_i \equiv \frac{TV_\infty}{Q\omega} = \left[\frac{1}{2} + \sqrt{\frac{1}{4} + \frac{\pi^2}{4J^2}\left(1 - \sqrt{1 - \frac{16C_T}{\pi^3}} \right)} \right]^{-1}$$

$$- \frac{J^2}{\pi^2} \left[\sqrt{1 + \frac{\pi^2}{J^2}\left(1 - \sqrt{1 - \frac{16C_T}{\pi^3}} \right)} - 1 \right] \tag{24}$$

By comparing Eqs. (23) and (24) with Eqs. (1) and (2), it can be shown that slipstream rotation increases the induced velocity and decreases the propulsive efficiency. However, it is not clear what the magnitudes of these effects are. To display the effect of slipstream rotation on propeller induced velocity, the solid lines in Fig. 2 show the percent error in Eq. (1) as compared with results predicted from Eq. (23). The dashed lines in Fig. 2 show a similar comparison for propulsive efficiency, based on results predicted from Eqs. (2) and (24).

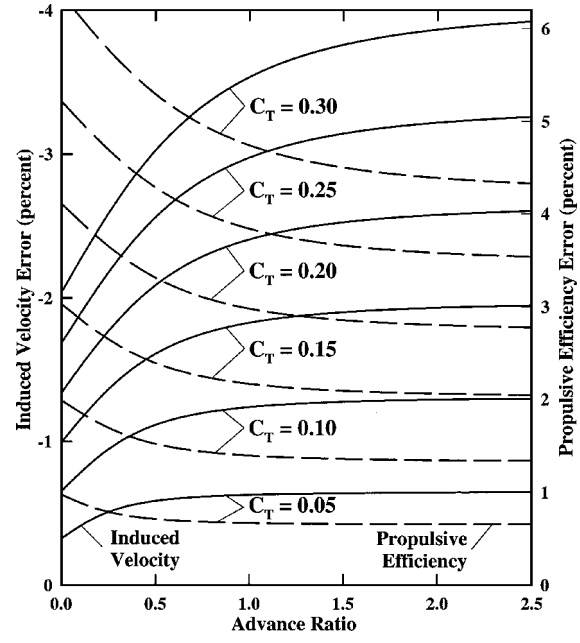

Fig. 2 Error in induced velocity (——) and propulsive efficiency (– – –) that results from neglecting slipstream rotation, as predicted by propeller momentum theory.

Conclusions

From Fig. 2 we see that the effect of slipstream rotation on induced velocity and propulsive efficiency, as predicted by propeller momentum theory, is on the order of 5% or less for the range of thrust coefficient and advance ratio that is normally encountered in airplane propellers. The induced velocity predicted by either Eq. (1) or Eq. (23) can be used with propeller blade element theory to replace the relation for induced velocity obtained from Goldstein's vortex theory.[2] The major difference between the induced velocity predicted from momentum theory and that predicted from vortex theory is that momentum theory predicts a zero circumferential component of induced velocity on the upstream side of the propeller. This is not true for vortex theory. In any case the effects of circumferential induced velocity are not large, particularly for lightly loaded propellers, and momentum theory provides some valuable insight into propeller performance with comparatively little effort. The major objection to classical propeller momentum theory has always been its failure to account for the rotation of the fluid within the slipstream. The analysis presented here has shown that the error in classical propeller momentum theory, which results from neglecting slipstream rotation, is small. It also provides a method to account for this rotation, if desired.

References

[1] McCormick, B. W., "Blade Element Theories," *Aerodynamics of V/STOL Flight*, Dover, New York, 1999, pp. 79–93.

[2] Goldstein, S., "On the Vortex Theory of Screw Propellers," *Proceedings of the Royal Society A*, Vol. 123, No. 792, 1929, pp. 440–465.

[3] Perkins, C. D., and Hage, R. E., "Propeller Charts," *Airplane Performance Stability and Control*, Wiley, New York, 1949, pp. 141–153.

[4] McCormick, B. W., "Classical Momentum Theory," *Aerodynamics of V/STOL Flight*, Dover, New York, 1999, pp. 73–79.

[5]McCormick, B. W., "Momentum Theory," *Aerodynamics, Aeronautics, and Flight Mechanics*, 2nd ed., Wiley, New York, 1995, pp. 291–297.

Active Control of Separation on a Wing with Oscillating Camber

David Munday* and Jamey Jacob†
University of Kentucky, Lexington, Kentucky 40506-0108

Nomenclature

c = chord length, 20.3 cm
f = actuation frequency, Hz
f^+ = reduced frequency, $f \cdot c/U$
Re = Reynolds number based on c
U = freestream velocity
α = angle of attack, deg

Introduction

LOW-REYNOLDS-NUMBER effects are significant in the aerodynamics of low-speed airfoils, aircraft intended to operate in low-density environments, and small-scale lifting surfaces such as insect and bird wings. Current aerodynamic applications include micro-aerial vehicles and unmanned aerial vehicles, as well as aircraft operating at high altitudes or low-density atmospheres other than Earth's.

The primary difficulty with the operation of a wing at low Reynolds number is that the flow over the suction surface encounters an adverse pressure gradient at a point at which the boundary layer is quite likely to still be laminar. Because a laminar boundary layer is incapable of negotiating any but the slightest adverse pressure gradient, the flow will inevitably separate. The separated flow then transitions to turbulence, entrains fluid, and reattaches to form a turbulent boundary layer. The resulting structure is the laminar separation bubble, which has been described by Lissaman.[1]

A number of different flow-control approaches have been investigated to reduce separation and improve efficiency at low Reynolds numbers.[2] Continuous blowing and sucking have long been shown to have pronounced effects. More recently, intermittent blowing and sucking in the form of synthetic jets have shown their effectiveness and suggest the presence of optimum values in the range of frequency inputs, which can translate to other oscillatory inputs.[3–5] Mechanical momentum transfer and acoustic excitation have also been explored.

The approach presented herein employs an adaptive wing.[6] Naturally, all practical wings are adaptive in the sense that they use actuators to alter lift coefficient by changing effective profile with a subsequent loss in efficiency. A truly adaptive wing, however, refers to an airfoil, which can change its profile to adapt optimally to flow conditions. Similar concepts have been explored in the past, such as the snap-through airfoil, which changes local airfoil camber by moving a flexible portion of the pressure surface[7] or the Defense Advanced Research Projects Agency "smart wing," which uses torsional elements to twist the wing.[8] Modern smart materials such as piezoelectric actuators offer great promise in the area of future stall control applications,[9] although simple mechanisms such as buzzing bars have also been shown to be adequate stall control devices.[10] The kind of adaptation, which is of interest here, is one in which the rate of actuation is rapid and might be able to respond quickly enough to arrest or limit the formation of laminar separation bubbles. At high Reynolds numbers the unsteady theory of Theodorsen[11] can be used to solve such problems (for an example, see Duffy et al.[12]), but at low Reynolds numbers where viscous forces are predominate there is no rigorous method to predict the unsteady effects of such rapid actuation and how it will alter separation.

Experiment

The adaptive wing design is based upon a static prototype design constructed by Pinkerton and Moses as a feasibility test for drag reduction.[13] A modular wing was constructed with a base profile of a NACA 4415. Each module has a recess cut in the upper surface into which a piezoelectric actuator is placed. The actuators are mounted at such an angle that they are even with the unrecessed airfoil section when at their smallest effective radius (when most curved). A thin plastic sheet is then placed over the actuator to smooth the profile, and then the entire assembly is wrapped in a latex membrane to hold it together and provide a seamless outer surface. When the actuator is displaced to its greatest effective radius (closest to being flat), it protrudes through the upper cross section. The plastic sheet and latex membrane smooth the upper surface, increasing the effective camber and moving the point of maximum thickness aft. The device has been more fully described elsewhere.[14]

Experiments with a circular-arc airfoil at low Reynolds number suggest that an airfoil with oscillating camber will produce a higher lift coefficient than the same airfoil at any fixed camber setting through separation control.[15] The present experiment attempts to extend this finding to airfoils of more ordinary and more efficient cross section. The current experiments were conducted with four wing modules, assembled to form a wing with a chord of 8 in. (203 mm) and a span of 13 in. (330 mm), giving an aspect ratio of 1.6. This wing was mounted in an 8×16-in. (203×406 mm) test section in a low-speed low-turbulence wind tunnel. Smoke-wire flow visualization as described in Batill and Mueller is used to mark the outer boundary of separated flow.[16] Displacement of the actuators was measured in situ with a Keyance LK-501 laser displacement sensor. These measurements are accurate to within $\pm 5\%$ at all frequencies across the range of interest.

Results

Flow visualization at $Re = 2.5 \times 10^4$ and 5.0×10^4 clearly shows large separated flow over the wing with the actuator static ($f^+ = 0$). This is expected at low speeds with a NACA 4415 profile, which is not designed for low-Reynolds-number flight. When the actuator is oscillating, the size of the separated flow is greatly reduced. Figure 1 shows images of the flow visualization for $Re = 2.5 \times 10^4$ at two different angles of attack for both uncontrolled and controlled runs where $f^+ = 0$ and $f^+ > 0$, respectively. From the recorded images the size of the separated region at 70% of chord was measured normal to the surface of the foil by determining the distance from the airfoil surface to the mean location of the first smoke streakline. These measurements are presented in Figs. 2 and 3. The instrumental error in these measurements amounts to ± 0.2 mm or far less than 1% of chord. This is dwarfed by the statistical error, which can best be inferred from examining the scatter in the dynamic data (variation in streakline location). The overall error, then, is within $\pm 1\%$ of chord.

The static measurements refer to those where the actuator was kept in a stationary state at a number of predetermined positions. For these an increase in separation as angle of attack increases is seen, which is what would be expected. An increase in separation as Reynolds number decreases is also seen. This is also as one would expect. The main purpose of the static measurements was to provide a direct comparison to the dynamic measurements. To that end the minimum size observed is the value used in Fig. 4, which represents a best-case scenario for separated flow over an unactuated airfoil.

Received 7 July 2001; revision received 3 August 2001; accepted for publication 9 November 2001.

*Graduate Student, Department of Mechanical Engineering; munday@engr.uky.edu. Member AIAA.
†Assistant Professor, Department of Mechanical Engineering; jdjacob@uky.edu. Senior Member AIAA.